XLVI CILAMCE
VITÓRIA - ES - BRAZIL - 2025
XLVI IBERO-LATIN AMERICAN CONGRESS ON COMPUTATIONAL METHODS IN ENGENEERING

Numerical Modeling Hierarchy for Tensile Testing of SAE 1020 Steel Specimens

Gabriel D. Dehete-Many[1], Guilherme E. Sousa[2], Claudio P. Junior[3], Rafael M. Ferro[4], Rodolfo G. M. de Andrade[5]

[1]*Master's student in Metallurgical and Materials Engineering, Federal Institute of Espírito Santo - Vitória Campus*
Av. Vitória, 1729, 29040-780, Jucutuquara, Vitória-ES, Brazil
gabriel_delboni@hotmail.com
[2]*Undergraduate in Mechanical Engineering, Federal Institute of Espírito Santo - Vitória Campus*
Av. Vitória, 1729, 29040-780, Jucutuquara, Vitória-ES, Brazil
gui1704esousa@gmail.com
[3]*Mechanics Coordination, Federal Institute of Espírito Santo - Vitória Campus*
Av. Vitória, 1729, 29040-780, Jucutuquara, Vitória-ES, Brazil
claudiop@ifes.edu.br
[4]*Coordination of Mechanical Engineering, Federal Institute of Espírito Santo - Aracruz Campus*
Av. Morobá, 248, 29192-733, Marobá, Aracruz-ES, Brazil
rafael.ferro@ifes.edu.br
[5]*Coordination of Buildings, Federal Institute of Espírito Santo - Vitória Campus*
Av. Vitória, 1729, 29040-780, Jucutuquara, Vitória-ES, Brazil
rodolfo.andrade@ifes.edu.br

Abstract. This study presents a hierarchical approach to finite element modeling for tensile testing of SAE 1020 steel specimens, according to ISO 6892-1. The objective is to analyze the convergence between analytical, numerical, and experimental results, balancing physical accuracy with computational efficiency. The hierarchy is constructed through the progressive refinement of numerical models using the 'PLANE182', 'SHELL181', and 'SOLID186' elements in ANSYS with linear analysis. The models are compared with an analytical solution based on the Theory of Strength of Materials and with experimental data obtained on a universal testing machine. The results show that all numerical models converge to values with an error of less than 1% compared to the analytical solution, with the 'PLANE182' elements being the most computationally efficient. The experimental results, however, exhibit greater dispersion and deviate by approximately 22% from the analytical value, highlighting challenges related to material variability and boundary condition uncertainties. The proposed method effectively demonstrates how modeling hierarchies can support decision-making in engineering environments, optimizing simulation accuracy, time, and computational resources.

Keywords: Numerical model hierarchy, Numerical modeling, Finite element method, Tensile testing, Mesh refinement.

1 Introduction

Computational modeling is an essential field for technological development in various engineering fields. As a result, the expansion of these models enables the resolution of complex physical-mathematical formulations, enabling the simulation of phenomena that, in many cases, would be impossible to reproduce experimentally or analytically. These resources provide a representation of a real system, capable of predicting its behavior and aiding in the optimization of a project, reducing costs and facilitating the project's implementation [1, 2].

However, this process can require high computational costs and can demand significant simulation time, especially when dealing with multidimensional, nonlinear, or problems dependent on multiple physical variables. This is problematic, even with the advancement in processing capacity resulting from hardware advances [1, 3].

Furthermore, the accuracy of the results is also directly related to the quality of the input data, the refinement of the computational mesh, and the robustness of the algorithms used. Hence, striking a balance between physical fidelity and numerical efficiency is one of the main challenges of contemporary computational modeling, and mastering it becomes essential for engineers and researchers seeking to optimize their solutions [4, 5].

In this context, hierarchy analysis between numerical and computational models emerges, aiming to relate the achieved accuracy to the computational resources required, based on convergence criteria to the desired real result. This operation aims to achieve the lowest processing cost, capable of achieving a result closest to the real behavior, while also minimizing execution time [6].

This research applied the Finite Element Method (FEM) to the tensile test of a flat, thin element made of SAE 1020 steel, using the student edition of Ansys Mechanical 2025 R1 software. Its objective was to analyze the convergence of the numerical results compared to: (i) the result obtained through analytical calculations; and (ii) the experimental result, from tests performed in the mechanical testing laboratory of the IFES Vitória Campus.

2 Method

The method was developed based on the pre-defined material examined, a 2 mm thick SAE 1020 steel plate, and the type of mechanical test employed, which was a tensile test performed at room temperature. Consequently, the ABNT NBR ISO 6892-1 standard, which specifies the procedures for tensile testing on metallic materials, was adopted to designate the geometry of the test specimen and the boundary conditions of the test [7].

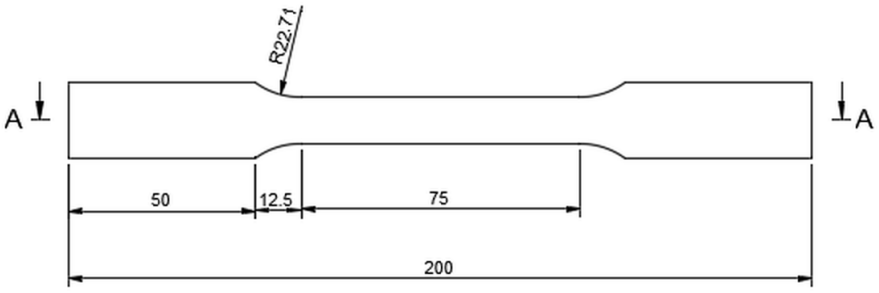
Based on these parameters, the geometric modeling of the specimen was established, along with the respective definition of the applied forces. Furthermore, an analytical approach to the model was also performed, which served as a comparative basis for the numerical simulations.

However, the modeling hierarchy was defined during the numerical analysis stage, in which the element type and mesh density used were varied in order to assess their impact on the accuracy of the solution.

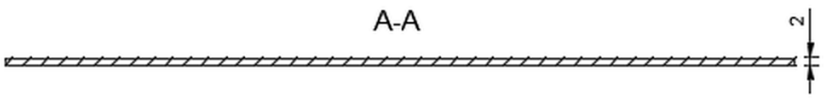
The methodology followed a structured sequence, beginning with: initially, the type of test, the corresponding standard, and, based on this, the geometry and boundary conditions were defined. Next, geometric modeling and simulation of boundary conditions were carried out, testing different types and densities of mesh elements in the same numerical model, with the aim of verifying the convergence of numerical solutions in relation to the analytical and experimental results.

2.1 Geometry and Geometric Modeling

The geometry of the test specimens, which included both physical specimens and the analytical and numerical models, followed the recommendations of the ABNT NBR ISO 6892-1 standard for flat products with thicknesses between 0.1 mm and 3 mm [7]. Figure 1 shows the dimensions of the specimen built using the student license of Autodesk Inventor Professional 2025 [8].



(a) Top view

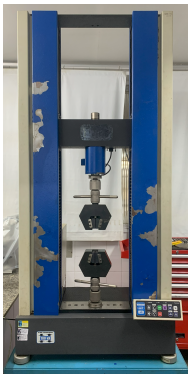


(b) Cut A-A

Figure 1. Test specimen.

2.2 Tensile Test

The tensile test at room temperature, in accordance with ABNT NBR ISO 6892-1, used the EMIC DL/10000 universal press [9] and a clip-on axial extensometer with a 50 mm measuring base, shown in Figure 2.



(a) EMIC DL/10000 Universal Testing Machine



(b) Extensometer coupled to the test piece

Figure 2. Tensile test arrangement with extensometer.

During the test, a speed of 5 mm/min was applied at a temperature of approximately 22°C, using 11.47% of the capacity of the 10,000 kgf load cell at EMIC [10, 11]. The specimens were fixed to the press using self-locking wedge-shaped clamps, aligned to prevent fluctuations in the values obtained during the displacement of the upper wedge [12].

2.3 Analytical Approach

In the analytical study of specimen deformation, the following conditions were adopted: (i) homogeneous body; (ii) uniaxial and continuous deformation in the length direction; and (iii) constant force along the length.

From these premises, the deformation (ϵ) was calculated from the ratio between the elongation (ΔL) and the initial length (L_0) of the specimen, as expressed in Equation 1 [13]:

$$\epsilon = \frac{\Delta L}{L_0} = \frac{1}{L_0}\int_0^{L_0} \epsilon(x)dx = \frac{1}{L_0}\int_0^{L_0} \left(\frac{F}{E \cdot 2 \cdot b(x) \cdot e}\right) dx \tag{1}$$

Where the definite integral can be simplified by segmenting suitable sub-intervals of the domain, as shown in Figure 3.

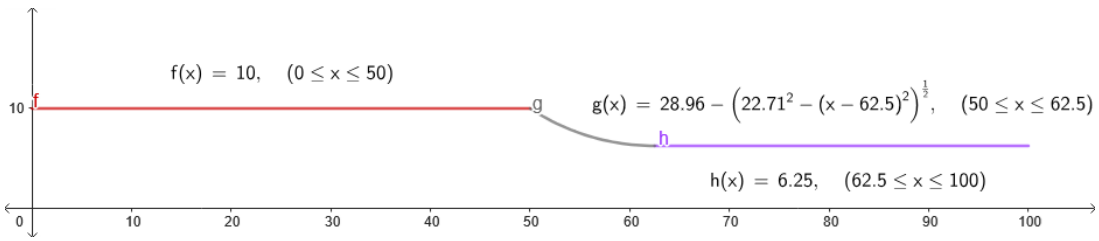


Figure 3. Partial mathematical representation of half-width of the specimen: $b(x)$

As a result, the following decomposition was obtained represented in Equation 2:

$$\epsilon = \frac{1}{L_0}\left[2\int_0^{50}\left(\frac{F}{E \cdot 2 \cdot f(x) \cdot e}\right)dx + 2\int_{50}^{62.5}\left(\frac{F}{E \cdot 2 \cdot g(x) \cdot e}\right)dx + 2\int_{62.5}^{100}\left(\frac{F}{E \cdot 2 \cdot h(x) \cdot e}\right)dx\right] \tag{2}$$

Therefore, along with the respective function in the interval, simply replace the parameters considered constant—force ($F = 5.87\ kN$), Young's modulus ($E = 212.4\ GPa$), initial length ($L_0 = 200\ mm$), and thickness ($e = 2\ mm$)—and solve the elementary integrals.

It is also worth noting that the data used in this approach are the same as those used in the numerical simulation, Subsection 2.4, from the Ansys database for annealed 1020 carbon steel.

Thus, 80% of the material's yield stress was used to ensure that its response remained in the elastic regime. Given that, the modulus of elasticity and deformation do not vary significantly in this range, even for materials that have undergone different heat treatments [14–16].

2.4 Numerical Modeling

Ansys Mechanical software, along with the Ansys Workbench 2025 R1 development environment and its processing modules, enabled the application of the FEM.

These modules provide a workflow in which the required analysis is initially defined, which in this case is static structural analysis, followed by the material used and the import of the respective geometry [17].

Based on the definition of the preprocessing modules, the appropriate mesh elements are generated and the relevant boundary conditions are introduced (Figure 4). Upon completion, the solution is obtained and the required result is displayed, which in this case is the strain.

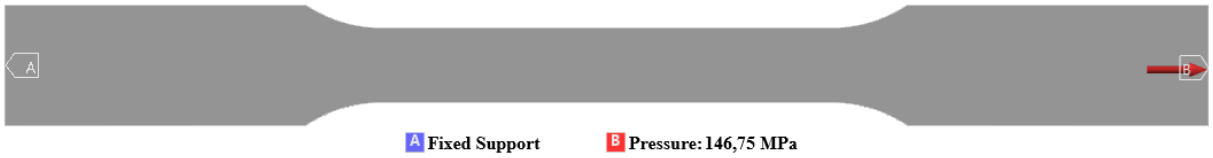


Figure 4. Linear Static Structural Analysis Boundary Conditions

The numerical hierarchy was implemented during the design phase of the mesh elements. In this model, input factors are progressively adjusted, starting with configurations using tens of elements and progressing to those with thousands.

Thus, three element types were used ('PLANE182', 'SHELL181', and 'SOLID186'), with mesh densities varied by adjusting element sizes. This process started with the largest element size required for FEM application in Ansys, down to the finest mesh resolution allowed by the student edition's numerical limitations.

3 Results

3.1 Experimental

Figure 5 shows the specific strain values (μS) obtained in the tensile tests for two groups of specimens with similar characteristics. In the group with 3 test specimens, data dispersion is low, with the median close to 980 μS and the lower and upper quartiles between 940 and 1040 μS, respectively. The overall range of variation is narrow, with minimum and maximum values close to 920 μS and 1070 μS. These results indicate high repeatability and consistency among the specimens tested in this group.

In contrast, the group with 8 specimens presents greater variability and a larger number of observations. The median is around 1130 μS, and the quartiles extend approximately from 1050 to 1270 μS, reflecting a widening of the interquartile range. The minimum recorded deformation remains close to 920 μS, while the maximum exceeds 1550 μS. This increased dispersion may be associated with material heterogeneity, variations in the test specimen manufacturing process, or even fluctuations in experimental conditions (boundary conditions).

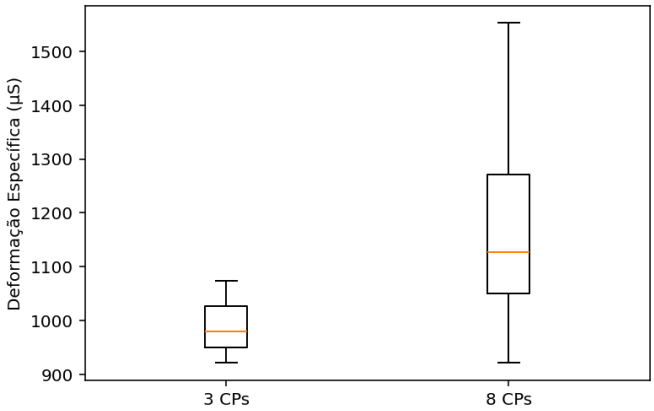


Figure 5. Comparison between groups of specimens subjected to tensile testing.

3.2 Numerical convergence

Figure 6 presents the results obtained in the simulations for the three element types, comparing them with analytical and experimental results. In this simulation, the specimen deformation is related to the number of mesh elements for each type of element introduced. Therefore, it is possible to observe that: (i) the three elements converge to the same numerical solution of 884.2 μS; (ii) the numerical solution varies 0.71% from the analytical result of 878 μS; (iii) the experimental result of 1070 μS varies 21.87% from the analytical result; (iv) the elements 'PLANE182' and 'SOLID186' converge with fewer iterations or mesh refinements than the element 'SHELL181'.

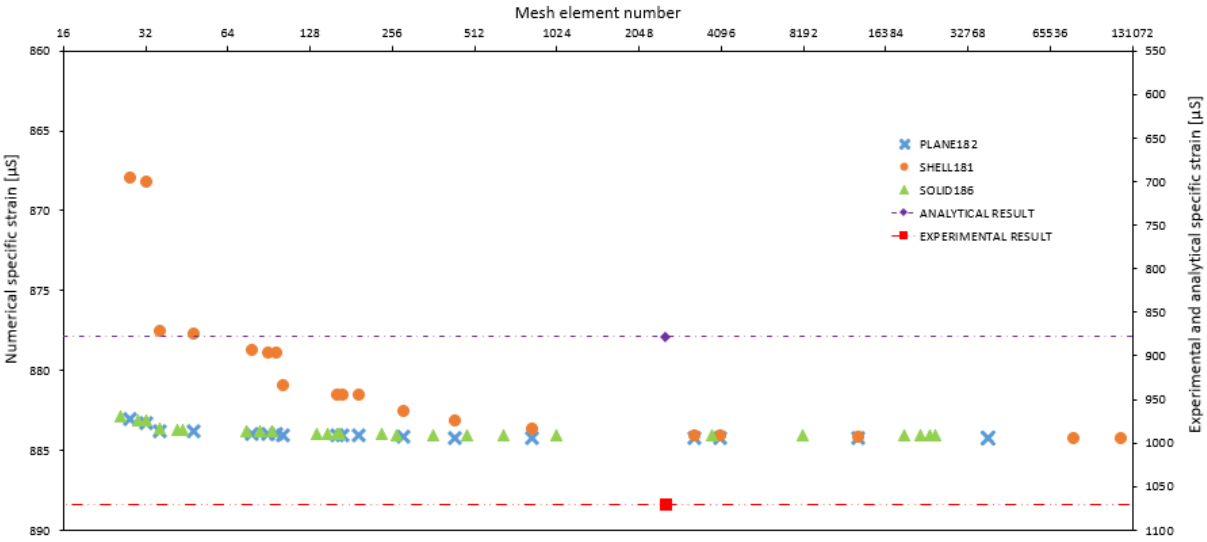


Figure 6. Convergence results for 'PLANE182', 'SHELL181', and 'SOLID186' elements compared to analytical and experimental benchmarks

In summary, all element types—from the simplified two-dimensional 'PLANE182', through 'SHELL181' for thin surfaces, to the three-dimensional 'SOLID186'—showed convergence close to the analytical result. However, the experimental result differed from the analytical result, possibly due to: (i) material supplied without guaranteed chemical composition; (ii) maintenance and calibration outside the recommended frequency; (iii) variations in the preparation of the specimens; (iv) fluctuations in the experimental boundary conditions.

Finally, Figure 7 shows the processing time for each simulation related to the type and number of mesh elements. Thus, the graph shows the increase in time relative to the increase in the required computational cost. The significant increase in the interval between elements 'PLANE182' and 'SHELL181' compared to 'SOLID186' resulted from the use of different machines in the simulations, likely due to differences in hardware performance

or system workload during the simulation runs or holding less data volume at the time of the simulations.

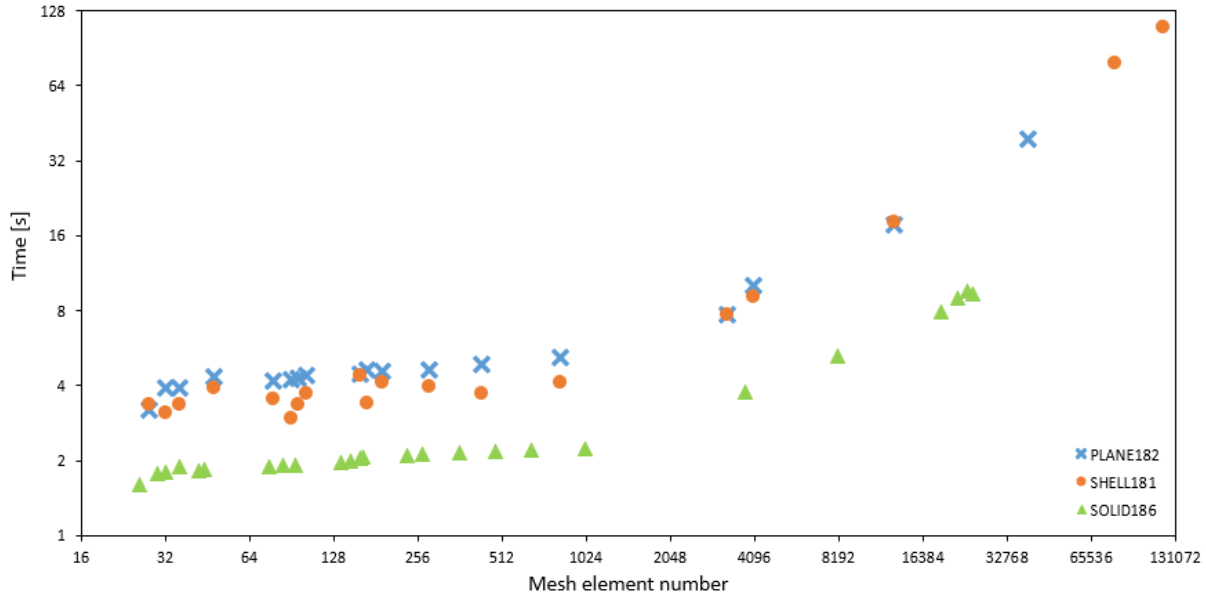


Figure 7. Processing time for each mesh element

4 Conclusion

The application of a hierarchy of numerical models to simulate tensile testing on SAE 1020 steel test specimens proved to be an efficient strategy for balancing physical fidelity and computational resource savings. The comparison between the results obtained through analytical, numerical, and experimental models showed that, even with different mesh types and densities, the numerical models were able to converge with relative errors below 1%.

The progressive use of the 'PLANE182', 'SHELL181', and 'SOLID186' elements allowed us to evaluate the impact of element complexity on the accuracy of the results and processing time. It was observed that less complex elements, such as 'PLANE182', are capable of providing satisfactory results with lower computational and time costs, making them ideal for preliminary analyses. In summary, the hierarchy proposed in this study demonstrated relevant information regarding accuracy, simulation time, and computational cost, making it suitable for supporting decision-making in engineering environments.

Furthermore, it is also important to consider the limitations of experimental tests, such as material variability and boundary conditions. Given the discrepancy between the experimental results and others, future work could incorporate models with material properties obtained directly by spectrometry and metallographic characterization, or tests performed with greater regulatory compliance, to increase the fidelity of the overall analysis.

Acknowledgements. We thank IFES and PROPEMM for their institutional support; CAPES for the scholarship (Process No. 88887.983267/2024-00); FAPES and CNPq for their support via PRONEM (Announcement 06/2019, T.O. 502/2020, SIAFEM 220-765DF); and everyone who contributed to this work.

Authorship statement. The authors hereby confirm that they are the sole liable persons responsible for the authorship of this work, and that all material that has been herein included as part of the present paper is either the property (and authorship) of the authors, or has the permission of the owners to be included here.

References

[1] A. A. Filho. *Elementos finitos: A base da tecnologia CAE: Análise dinâmica*. Editora Érica - Sob Demanda, 2009.

[2] J. Krzywanski, M. Sosnowski, K. Grabowska, A. Zylka, L. Lasek, and A. Kijo-Kleczkowska. Advanced computational methods for modeling, prediction and optimization—a review. *Materials*, vol. 17, pp. 3521, 2024.

[3] A. Sikirica, L. Grbčić, M. Alvir, and L. Kranjčević. Computational efficiency assessment of adaptive mesh refinement for turbulent jets in crossflow. *Mathematics*, vol. 10, 2022.

[4] M. Calder, C. Craig, D. Culley, de R. Cani, C. A. Donnelly, R. Douglas, B. Edmonds, J. Gascoigne, N. Gilbert, C. Hargrove, D. Hinds, D. C. Lane, D. Mitchell, G. Pavey, D. Robertson, B. Rosewell, S. Sherwin, M. Walport, and A. Wilson. Computational modelling for decision-making: where, why, what, who and how. *Royal Society Open Science*, vol. 5, n. 6, pp. 172096, 2018.

[5] Z. Boz, F. Erdogdu, and M. Tutar. Effects of mesh refinement, time step size and numerical scheme on the computational modeling of temperature evolution during natural-convection heating. *Journal of Food Engineering*, vol. 123, pp. 8–16, 2014.

[6] N. Parvez, S. N. Amjad, M. K. Dey, and C. R. Picu. Methodological aspects and mesh convergence in numerical analysis of athermal fiber network material deformation. *Fibers*, vol. 12, 2024.

[7] Associação Brasileira de Normas Técnicas (ABNT). Materiais metálicos — ensaio de tração. parte 1: Método de ensaio em temperatura ambiente. Norma Brasileira ABNT NBR ISO 6892-1:2024. Equivalente à ISO 6892-1:2019. Rio de Janeiro: ABNT, 79 p., 2024.

[8] Autodesk, Inc. *Autodesk Inventor*. Versão estudantil, 2025.

[9] EMIC Equipamentos e Sistemas de Ensaio Ltda. *Manual da Linha DL: Equipamento Modelo DL 5000/10000*. São José dos Pinhais, PR. Inclui Manual de Apresentação, Manual de Instalação, Programa Tesc EMIC e Instruções para Realização de Ensaios, s.d.

[10] Associação Brasileira de Normas Técnicas (ABNT). Materiais metálicos — calibração e verificação de máquinas de ensaio estático uniaxial. parte 1: Máquinas de ensaio de tração/compressão. Norma Brasileira ABNT NBR ISO 7500-1:2023. Equivalente à ISO 7500-1:2018. Rio de Janeiro: ABNT, 19 p., 2023.

[11] Associação Brasileira de Normas Técnicas (ABNT). Materiais metálicos — calibração de sistemas extensométricos usados em ensaios uniaxiais. Norma Brasileira ABNT NBR ISO 9513:2013. Equivalente à ISO 9513:2012. Rio de Janeiro: ABNT, 47 p., 2013.

[12] ASTM International. Standard practice for verification of testing frame and specimen alignment under tensile and compressive axial force application. ASTM Standard E1012-19, 2019.

[13] J. T. DeWolf, D. F. Mazurek, F. P. Beer, and E. R. J. Jr. *Mecânica dos Materiais - 8. ed.* McGraw Hill Brasil, 2021.

[14] S. Dewangan. Analysis of property variation in aisi 1020 steel after heat treatment. *AIP Conference Proceedings*, vol. 2341, n. 1, pp. 040025, 2021.

[15] S. Dewangan, N. Mainwal, M. Khandelwal, and P. S. Jadhav. Performance analysis of heat treated aisi 1020 steel samples on the basis of various destructive mechanical testing and microstructural behaviour. *Australian Journal of Mechanical Engineering*, vol. 20, n. 1, pp. 74–87, 2022.

[16] A. Villuendas, J. Jorba, and A. Roca. Variación del módulo de young con el tratamiento térmico en aceros al carbono hipoeutectoides. *Revista de Metalurgia (Madrid)*, vol. Vol. Extraordinario, pp. 46–52. Licença Creative Commons 3.0 España (by-nc), 2005.

[17] ANSYS Inc. *Ansys Mechanical User's Guide*. Canonsburg, PA. Versão estudantil, 2021.